2006

Oxalic acid in clear and cloudy atmospheres: Analysis of data from International Consortium for Atmospheric Research on transport and transformation 2004

Oxalic acid in clear and cloudy atmospheres: Analysis of data from International Consortium for Atmospheric Research on Transport and Transformation 2004

Armin Sorooshian,[1] Varuntida Varutbangkul,[1] Fred J. Brechtel,[1,2] Barbara Ervens,[3,4] Graham Feingold,[5] Roya Bahreini,[1,6] Shane M. Murphy,[1] John S. Holloway,[5] Elliot L. Atlas,[7] Gintas Buzorius,[8] Haflidi Jonsson,[8] Richard C. Flagan,[1] and John H. Seinfeld[1]

Received 10 November 2005; revised 11 February 2006; accepted 22 March 2006; published 26 August 2006.

[1] Oxalic acid is often the leading contributor to the total dicarboxylic acid mass in ambient organic aerosol particles. During the 2004 International Consortium for Atmospheric Research on Transport and Transformation (ICARTT) field campaign, nine inorganic ions (including SO_4^{2-}) and five organic acid ions (including oxalate) were measured on board the Center for Interdisciplinary Remotely Piloted Aircraft Studies (CIRPAS) Twin Otter research aircraft by a particle-into-liquid sampler (PILS) during flights over Ohio and surrounding areas. Five local atmospheric conditions were studied: (1) cloud-free air, (2) power plant plume in cloud-free air with precipitation from scattered clouds overhead, (3) power plant plume in cloud-free air, (4) power plant plume in cloud, and (5) clouds uninfluenced by local pollution sources. The aircraft sampled from two inlets: a counterflow virtual impactor (CVI) to isolate droplet residuals in clouds and a second inlet for sampling total aerosol. A strong correlation was observed between oxalate and SO_4^{2-} when sampling through both inlets in clouds. Predictions from a chemical cloud parcel model considering the aqueous-phase production of dicarboxylic acids and SO_4^{2-} show good agreement for the relative magnitude of SO_4^{2-} and oxalate growth for two scenarios: power plant plume in clouds and clouds uninfluenced by local pollution sources. The relative contributions of the two aqueous-phase routes responsible for oxalic acid formation were examined; the oxidation of glyoxylic acid was predicted to dominate over the decay of longer-chain dicarboxylic acids. Clear evidence is presented for aqueous-phase oxalic acid production as the primary mechanism for oxalic acid formation in ambient aerosols.

Citation: Sorooshian, A., et al. (2006), Oxalic acid in clear and cloudy atmospheres: Analysis of data from International Consortium for Atmospheric Research on Transport and Transformation 2004, *J. Geophys. Res.*, *111*, D23S45, doi:10.1029/2005JD006880.

1. Introduction

[2] Dicarboxylic acids are ubiquitous in atmospheric aerosols [*Norton et al.*, 1983; *Kawamura and Kaplan*, 1987; *Kawamura and Ikushima*, 1993; *Khwaja et al.*, 1995; *Kawamura et al.*, 1995, 1996, 2003, 2005; *Liu et al.*, 1996; *Kawamura and Sakaguchi*, 1999; *Limbeck and Puxbaum*, 1999; *Kerminen et al.*, 2000; *Poore*, 2000; *Puxbaum et al.*, 2000; *Pakkanen et al.*, 2001; *Rohrl and Lammel*, 2001; *Yao et al.*, 2002a, 2004; *Salam et al.*, 2003a, 2003b; *Crahan et al.*, 2004; *Shantz et al.*, 2004; *Yu et al.*, 2005] and cloud droplets [*Weathers et al.*, 1988; *Limbeck and Puxbaum*, 2000; *Hegg et al.*, 2002; *Loflund et al.*, 2002; *Crahan et al.*, 2004]; however, the physical and chemical routes by which these compounds form and are sequestered in particulate matter are not fully understood. The presence of dicarboxylic acids in pure and mixed aerosols may affect both deliquescence relative humidity and hygroscopic

[1]Departments of Environmental Science and Engineering and Chemical Engineering, California Institute of Technology, Pasadena, California, USA.
[2]Also Brechtel Manufacturing Inc., Hayward, California, USA.
[3]Department of Atmospheric Science, Colorado State University, Fort Collins, Colorado, USA.
[4]Also at Earth System Research Laboratory/Chemical Sciences Division, NOAA, Boulder, Colorado, USA.
[5]Earth System Research Laboratory/Chemical Sciences Division, NOAA, Boulder, Colorado, USA.
[6]Now at Earth System Research Laboratory/Chemical Sciences Division, NOAA, Boulder, Colorado, USA.
[7]Division of Marine and Atmospheric Chemistry, Rosenstiel School of Marine and Atmospheric Science, University of Miami, Miami, Florida, USA.
[8]Center for Interdisciplinary Remotely Piloted Aircraft Studies, Naval Postgraduate School, Marina, California, USA.

0148-0227/06/2005JD006880

behavior [*Cruz and Pandis*, 1998; *Brooks et al.*, 2002; *Kumar et al.*, 2003]; the radiative impact of particles containing dicarboxylic acids depends on their effectiveness in absorbing water as a function of relative humidity.

[3] Oxalic acid, $(COOH)_2$, a by-product of fossil fuel combustion, biomass burning, and biogenic activity, has been shown in many studies to be the most abundant dicarboxylic acid in tropospheric aerosols [*Kawamura and Kaplan*, 1987; *Kawamura and Ikushima*, 1993; *Kawamura et al.*, 1995, 1996, 2003, 2005; *Liu et al.*, 1996; *Kawamura and Sakaguchi*, 1999; *Kerminen et al.*, 2000; *Poore*, 2000; *Loflund et al.*, 2002; *Yao et al.*, 2002a, 2004; *Salam et al.*, 2003a, 2003b; *Crahan et al.*, 2004; *Yu et al.*, 2005]. Studies have suggested, however, that primary sources of particulate oxalic acid cannot account for ambient levels that have been measured globally [*Poore*, 2000; *Warneck*, 2003; *Yao et al.*, 2004; *Yu et al.*, 2005].

[4] Oxalate, the anion of oxalic acid, is typically detected by analytical techniques such as ion chromatography (IC). In some observations, oxalate-containing particles show two distinct accumulation modes at 0.2 ± 0.1 μm and 0.7 ± 0.2 μm, with the larger mode being associated with SO_4^{2-} [*Kerminen et al.*, 1999, 2000; *Kalberer et al.*, 2000; *Yao et al.*, 2002b, 2003; *Crahan et al.*, 2004]. Suggested oxalate formation mechanisms in the fine particulate mode include in-cloud processing, oxidation of gaseous species followed by condensation, and aerosol surface reactions [*Kawamura and Ikushima*, 1993; *Faust*, 1994; *Chebbi and Carlier*, 1996; *Blando and Turpin*, 2000; *Yao et al.*, 2002b, 2003; *Mochida et al.*, 2003; *Turekian et al.*, 2003]. *Crahan et al.* [2004] measured in a coastal marine environment the air-equivalent concentrations of SO_4^{2-} and oxalate in cloudwater as approximately two and three times greater, respectively, than concentrations measured below cloud. They also detected glyoxylic acid, an intermediate in aqueous-phase oxalate production [*Leitner and Dore*, 1997], in cloudwater samples. On the basis of data from the literature and results from their own study, *Yu et al.* [2005] argue that a dominant in-cloud pathway can explain the close correlation between SO_4^{2-} and oxalate.

[5] During the 2004 International Consortium for Atmospheric Research on Transport and Transformation (ICARTT) study, measurements made by surface, airborne, and satellite platforms focused on examining the nature of air masses in the northeastern United States, the western Atlantic Ocean, and the Maritime Provinces of Canada. In August 2004, the Center for Interdisciplinary Remotely Piloted Aircraft Studies (CIRPAS) Twin Otter (TO), based at Hopkins International Airport in Cleveland, Ohio, participated in the ICARTT field campaign. The focus of the CIRPAS participation was to study aerosol and cloud condensation nuclei (CCN) physics and chemistry.

[6] The goal of the present work is to elucidate oxalic acid formation in the atmosphere. We analyze airborne measurements of SO_4^{2-} and oxalate in different conditions in the atmosphere around Ohio during ICARTT. The majority of the oxalate measurements were made while sampling either droplet residuals (the particle remaining after a cloud droplet has evaporated) or the total aerosol in clouds (the sum of interstitial aerosol and droplet residuals). We investigate the correlation between SO_4^{2-} and oxalate, and the role of other organic acids in aqueous-phase production of oxalate. The relative contributions of different aqueous-phase reactions are examined, as well as the magnitude of SO_4^{2-} and oxalate mass production rates in cloud-processed air. Finally, we assess the extent to which these rates agree with those predicted by a cloud parcel model containing a state-of-the-art mechanism for aqueous-phase production of SO_4^{2-} and oxalate.

2. Twin Otter (TO) Research Aircraft

[7] Table 1 summarizes the instruments that were operated on the TO. Chemical composition data analyzed here were obtained by a particle-into-liquid sampler (PILS), which will be described below. A quadropole Aerodyne Aerosol Mass Spectrometer (AMS) [*Jayne et al.*, 2000] provided chemical composition data for nonrefractory aerosol species. Aerosol size distribution data (10–800 nm diameter) were obtained by a Caltech dual differential mobility analyzer (DMA) system [*Wang et al.*, 2003], also called the Dual Automated Classified Aerosol Detector (DACAD). An external Passive Cavity Aerosol Spectrometer Probe (PCASP, PMS, modified by DMT Inc.) and an external Forward Scattering Spectrometer Probe (FSSP, PMS, modified by DMT Inc.) provided cloud and aerosol size distributions for the following particle diameter ranges, respectively: 0.1 to 2.0 μm and 2.0 to 40.0 μm.

[8] The main inlet was the primary inlet supplying sample flow to all instruments anytime the TO was outside of clouds and sometimes when it was inside clouds. The main inlet of the TO uses two diffusers to decelerate air by a factor of ten before it is sent to the sampling instruments. *Hegg et al.* [2005] characterized the behavior of the TO inlet; they report that the transmission efficiency of the inlet under standard flight conditions for particle diameters less than 3.5 μm is near unity, decreasing for larger particles until 5.5 μm and above, where the transmission efficiency remains slightly in excess of 60%. This transmission efficiency persists for particle diameters up to 9 μm, the upper limit of the characterization tests. When used in clouds, the main inlet sampled the total aerosol, which included interstitial aerosol and residual particles from evaporated cloud droplets. Evidence that droplet residuals were being sampled through the main inlet during ICARTT included the detection of aqueous-phase precursors to oxalic acid.

[9] A counterflow virtual impactor (CVI) inlet was employed only in clouds. The CVI selectively samples cloud droplets larger than a cutoff diameter of 10 (±20%) μm by isolating them from the interstitial aerosol, by means of inertial impaction. During the time the CVI was used, sample flow was diluted and divided for supply only to the PILS, AMS, a particle soot absorption photometer (PSAP, Radiance Research Inc.), and a condensation particle counter (TSI CPC 3010), during which time, all other instruments still sampled air entering through the main inlet. The instruments behind the CVI sampled residual particles from evaporated cloud droplets. PILS concentrations reported during CVI sampling should be considered as the lower limit to their true value because of uncertainties in the CVI transmission efficiency.

3. PILS-IC Measurements

[10] The PILS-IC is a quantitative technique for measuring water-soluble ions, including inorganic and organic acid

Table 1. Twin Otter Payload Description

Instrument	Data
Condensation particle counter (CPC)[a]	aerosol number concentration
Cloud condensation nucleus counter (CCN)	cloud condensation nucleus number concentration at 3 supersaturations
Counterflow virtual impactor (CVI)	virtual impactor for isolating cloud droplets
Dual automated classified aerosol detector (DACAD)	submicrometer aerosol size distribution (10–800 nm) at low and high RH
Aerosol spectrometer probe (PCASP), aerodynamic particle sizer (APS), forward scattering spectrometer probe (FSSP), cloud and aerosol particle spectrometer (CAPS)	aerosol/cloud droplet size distribution (120 nm to 1.6 mm)
Aerodyne aerosol mass spectrometer (AMS)[a]	nonrefractory aerosol chemistry
Particle-into-liquid sampler (PILS)[a]	submicrometer aerosol chemistry (IC: inorganic and some organic acid ions)
Filters	bulk aerosol chemistry (FTIR: functional group analysis)
PSAP,[a] photoacoustic, SP2	soot absorption (multiwavelength/incandescence)
Miscellaneous navigational and meteorology probes	navigational data, temperature, dew point, RH, pressure, liquid water content, wind direction/speed, updraft velocity, etc.

[a]These are the only instruments that sampled air coming through the CVI inlet.

ions in aerosol particles. The PILS developed and used in this study (Brechtel Manufacturing Inc., www.brechtel.com) is based on the prototype design [*Weber et al.*, 2001] with key modifications, including integration of a liquid sample fraction collector and real-time control of the steam injection tip temperature [*Sorooshian et al.*, 2006]. Ambient air is sampled through a 1-micrometer cut-size impactor and a set of three denuders (URG and Sunset Laboratories) to remove inorganic and organic gases that may bias aerosol measurements. The two annular glass denuders (URG-2000-30 × 242-3CSS) used for removal of inorganic gases are coated with solutions of either 2% sodium carbonate or 2% phosphoric acid (for removal of acidic and basic gases, respectively) in a solution of 100 mL of Milli Q water, 80 mL of methanol, and 2 g of glycerol. The third denuder (Sunset Laboratory Inc.), composed of 15 thin carbon filter paper sheets (3.15 cm × 20.32 cm × 0.04 cm thick) with 0.2 cm gaps between them, removes organic gases. Sample air mixes with steam in a condensation chamber where rapid adiabatic mixing produces a high water supersaturation. Droplets grow sufficiently large to be collected by inertial impaction before being delivered to vials held on a rotating carousel. The contents of the vials are subsequently analyzed off-line using a dual IC system (ICS-2000 with 25 μL sample loop, Dionex Inc.) for simultaneous anion and cation analysis. A fraction of each liquid sample was frozen for future reanalysis with a longer IC program capable of better detection of organic acid ions.

[11] Nine inorganic ions (Na^+, NH_4^+, K^+, Mg^{2+}, Ca^{2+}, Cl^-, NO_2^-, NO_3^-, and SO_4^{2-}) and five organic acid ions (oxalate, malonate, glutarate, pyruvate, and glyoxylate) were measured during the field campaign. The limit of detection (LOD) for each ion was determined by running the lowest concentration standard detectable by the IC and using the average concentration plus three times the standard deviation (n = 50) to calculate the air-equivalent concentration of each ion. The LODs for the ions measured using the PILS-IC technique for this study are all below 0.1 μg/m^3, with the organic anions and SO_4^{2-} exhibiting LODs below 0.03 μg/m^3.

[12] Measurements presented for glyoxylate, pyruvate, and glutarate are derived from reanalyzing the stored liquid volumes (they were frozen for 13 months). It should be noted that all vials were spiked with 5 μL of dichloromethane prior to storage to prevent biological processing. The mass concentrations of SO_4^{2-}, NH_4^+, and oxalate from the original and reanalyzed vials were compared for flight 5 on 9 August 2004 to determine the magnitude of variability between the two batches (Table 2). The concentrations measured in the original vials for the three ions exceeded the reanalyzed concentrations by factors between 1.54 and 1.83, indicating that there was degradation of ion levels during storage; potential explanations for degradation include the freezing and thawing process, the interaction of the sample with the vial surface, and the effect of dichloromethane. The reported concentrations of glyoxylate, pyruvate, and glutarate should be viewed as a lower limit, assuming that their degradation rates were similar to those measured for SO_4^{2-}, NH_4^+, and oxalate.

4. Field Measurements

4.1. Field Data Summary

[13] The TO flight tracks for all twelve flights between 1 and 21 August 2004 are shown in Figure 1. Several flights focused on areas downwind of the Monroe Power Plant (Monroe County, Michigan) and the Conesville Power Plant (Coshocton County, Ohio), both of which are coal-burning plants. The following types of atmospheric conditions were encountered over the entire 12-flight mission: (1) cloud-free air, (2) power plant plume in cloud-free air with precipitation from scattered clouds overhead, (3) power plant plume in cloud-free air, (4) power plant plume in cloud, and (5) clouds uninfluenced by local pollution sources. Figure 2 illustrates the sampling strategy used by the TO during flights when atmospheric condition types 2 and 4 were encountered; the TO flew a number of horizontal transect legs perpendicular to the studied plume. Figure 2b represents the case of type 3 as well, but in the absence of precipitation. Data grouped in the two cloud cases were identified by elevated relative humidities (RH > 100%) and high liquid water content (LWC > 0.1 g/m^3). Plumes were

Table 2. Comparison of PILS Original (Old) and Reanalyzed (New) Vials From Flight 5 on 9 August 2004

	[Old]/[New]
SO_4^{2-} (n = 42) slope (R^2)	1.66 (0.84)
NH_4^+ (n = 38) slope (R^2)	1.54 (0.50)
Oxalate (n = 34) slope (R^2)	1.83 (0.50)

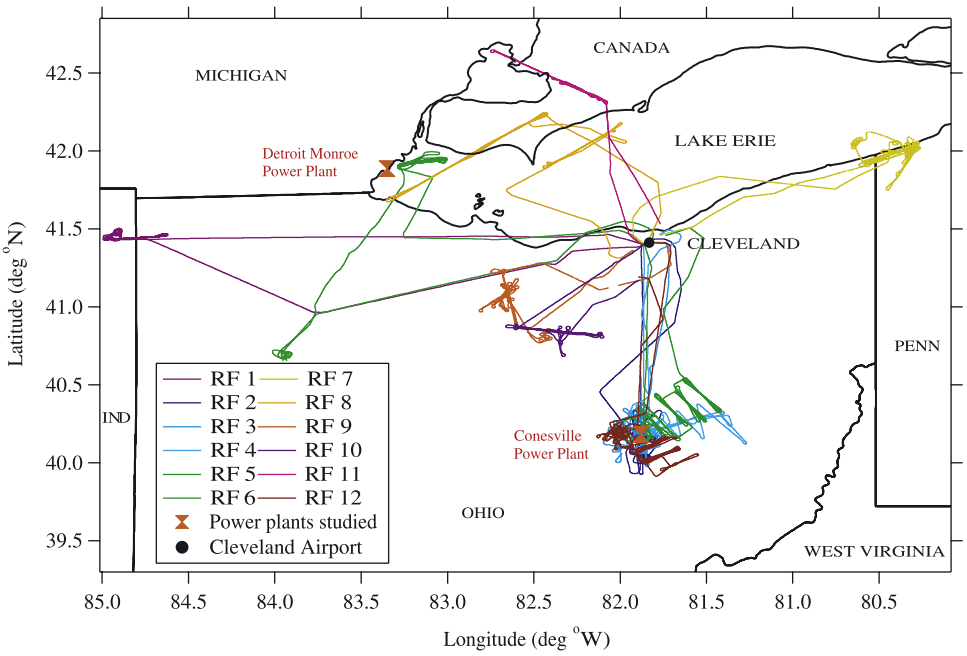

Figure 1. Twin Otter flight tracks during the ICARTT field study. RF refers to research flight.

identified by a dramatic increase in aerosol number concentration. It should be noted that the clouds uninfluenced by local pollution sources may have still been influenced by long-range transport of urban pollution.

[14] Characteristics of the clouds observed during flights 5 and 12 (9 and 21 August 2004, respectively), which are flights that will be examined in detail subsequently, are representative of the clouds encountered over the entire mission. The clouds were typically cumulus, which broadly encompasses stratocumulus, fair-weather cumulus, and cumulus congestus clouds, with thicknesses between 500 to 700 m. Cloud bases stayed on the order of 1500 m, and as the day proceeded, the tops grew from around 2000 m to between 2300 and 2700 m. Typical LWC vertical profiles indicate that there were slightly variable cloud base altitudes, and some entrainment drying. The LWC in clouds typically ranged from 0.1 to 1.0 g/m^3. The lower troposphere in the sampling region was marked by turbulence and convective instability. Soundings obtained on the ascents out of Cleveland show ambient and dew point temperatures tracing nearly straight lines to cloud base altitudes, reflecting instability and vigorous mixing. On average, vertical velocities near the cloud bases tended to be 1 m/s, increasing to 2 m/s during passes at higher levels in cloud.

[15] Figure 3 displays the vertical distribution of specific ions and the total mass measured through both inlets for the entire 12-flight mission. The mass concentrations of oxalate and SO_4^{2-} were evenly scattered at all altitudes up to about 2250 m, where they start to decrease, indicating the begin-

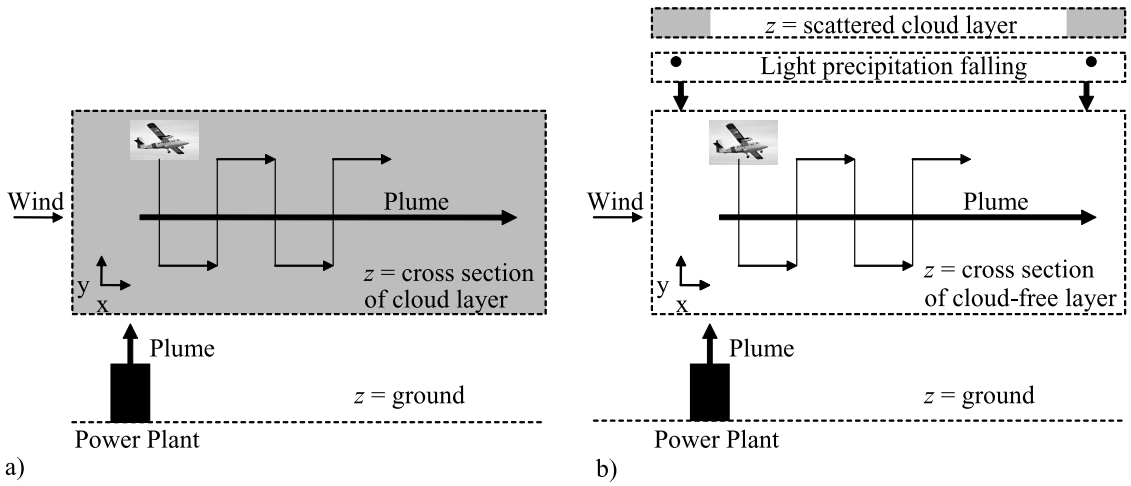

Figure 2. Simplified illustration of how the Twin Otter flew when it encountered two specific atmospheric conditions: (a) power plant plume in cloud and (b) power plant plume in cloud-free air with precipitation from scattered clouds overhead.

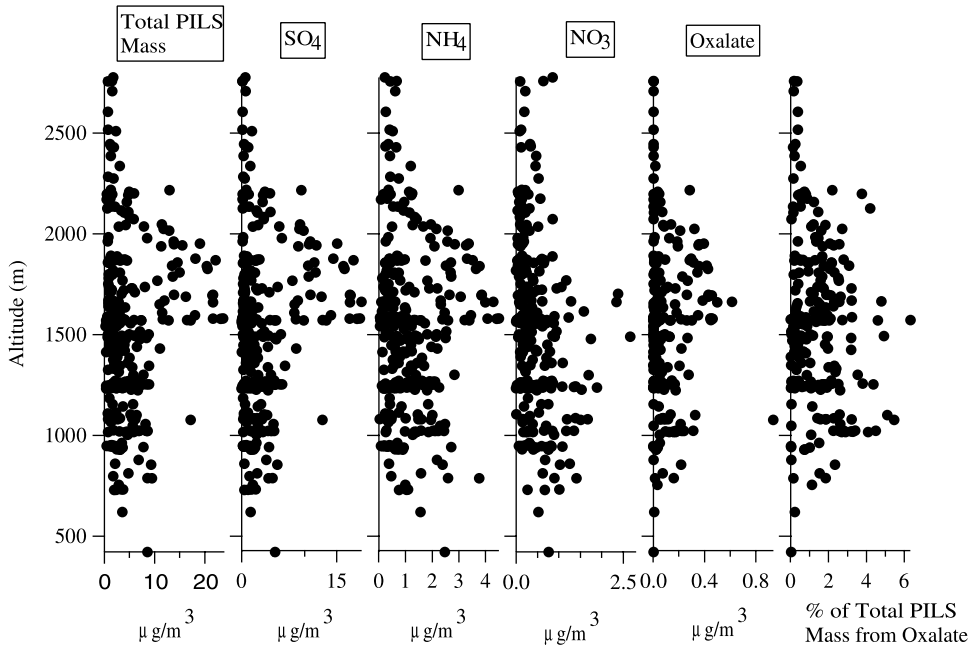

Figure 3. Vertical distribution of ions measured by the PILS during ICARTT.

ning of the free troposphere. Oxalate constituted up to 6.3% of the total water-soluble ionic mass as measured by the PILS. Table 3 shows the variation of the molar ratio of oxalate relative to three of the major inorganic ions for each atmospheric condition encountered and each inlet used. Overall, oxalate exhibits the strongest correlation with SO_4^{2-}, followed by NH_4^+ and then NO_3^-. Ammonium is correlated with SO_4^{2-}, since acidic sulfate-containing particles absorb ammonia. Oxalate and NO_3^- show a poor correlation, suggesting that these ions arise from different processes.

[16] The strongest correlations between SO_4^{2-} and oxalate were seen for the power plant plume in cloud category when droplet residual particles ($R^2 = 0.97$, $n = 11$) and the total aerosol ($R^2 = 0.77$, $n = 44$) were being individually sampled through the CVI and the main inlet, respectively. The next strongest correlation ($R^2 = 0.75$, $n = 54$) was observed when the total aerosol was measured in clouds uninfluenced by local pollution sources. During ICARTT, the highest single oxalate measurement (0.94 $\mu g/m^3$) occurred in a droplet residual sample from a power plant plume in cloud. Aerosol samples in that category represented the largest average oxalate (0.28 $\mu g/m^3$) and SO_4^{2-} (6.51 $\mu g/m^3$) loadings. Flight 5, the flight with the majority of the data points representing power plant plume in cloud, will be addressed in the next section.

[17] The lowest SO_4^{2-} and oxalate loadings occurred in cloud-free air (Figure 4); these samples showed no correlation between SO_4^{2-} and oxalate. Oxalate exceeded detection limits in only 24 out of 196 samples collected in cloud-free air. For total aerosol samples collected in power plant plume in cloud-free air, a moderate correlation between SO_4^{2-} and oxalate ($R^2 = 0.56$, $n = 18$) was observed only for the precipitation case, where oxalate levels exceeded 0.1 $\mu g/m^3$. In the absence of precipitation, the correlation was much lower ($R^2 = 0.21$, $n = 10$) and

Table 3. Molar Ratio of Oxalate Relative to Sulfate, Nitrate, and Ammonium[a]

Atmospheric Condition Type and Inlet (Number of Vials With Oxalate Above Detection Limits/Total Number of Vials)	SO_4^{2-} Slope (R^2)	NO_3^- Slope (R^2)	NH_4^+ Slope (R^2)
Clouds uninfluenced by local pollution sources			
CVI (34/131)	0.014 (0.37)	0.010 (0.15)	0.006 (0.24)
Main (54/92)	0.024 (0.75)	−0.007 (0.01)	0.015 (0.59)
Cumulative (88/223)	0.023 (0.71)	0.000 (0.00)	0.013 (0.55)
Power plant plume in cloud			
CVI (11/32)	0.083 (0.97)	−0.009 (0.00)	0.073 (0.45)
Main (44/79)	0.028 (0.77)	−0.110 (0.03)	0.026 (0.81)
Cumulative (55/111)	0.028 (0.82)	−0.031 (0.04)	0.026 (0.84)
Cloud-free air			
Main (24/196)	0.000 (0.00)	0.010 (0.08)	0.002 (0.17)
Power plant plume in cloud-free air			
Main (10/24)	0.015 (0.21)	0.011 (0.10)	0.011 (0.28)
Power plant plume in cloud-free air with precipitation from scattered clouds overhead			
Main (18/21)	0.051 (0.56)	0.031 (0.09)	0.024 (0.52)

[a]CVI samples correspond to cloud droplet residual particles; main inlet samples correspond to total aerosol, which includes a mixture of interstitial aerosol and droplet residuals in clouds.

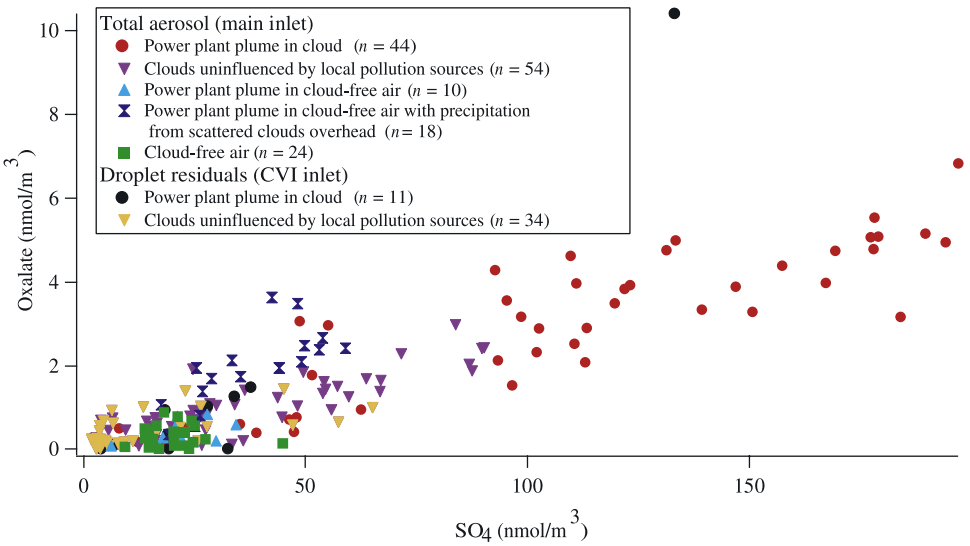

Figure 4. Oxalate and SO_4^{2-} molar concentrations for each atmospheric condition encountered. The total aerosol samples collected in cloud consist of a mixture of interstitial aerosol and droplet residuals.

oxalate levels were less than 0.1 μg/m^3. All samples representing power plant plume in cloud-free air with precipitation from scattered clouds overhead are from flight 4 on 8 August 2004, where oxalate constituted up to 5.1% of the water-soluble ionic mass, which corresponded to the vial with the maximum oxalate loading (0.33 μg/m^3). Table 3 shows that oxalate was measured in the greatest amount relative to SO_4^{2-} during this flight compared to all total aerosol samples from other atmospheric condition categories; however, no key aqueous-phase intermediates in oxalic acid formation were detected. Therefore we cannot preclude sources of oxalic acid other than cloud processing, such as gas-phase oxidation of parent organic species followed by condensation.

[18] As noted in the Introduction, previous studies have ruled out primary sources as the main formation mechanism for oxalic acid based on spatial and temporal characteristics [*Poore*, 2000; *Yao et al.*, 2004; *Yu et al.*, 2005]. If primary sources were responsible for observed oxalate levels, then comparable levels should have been measured in all of the aforementioned atmospheric conditions encountered. That the oxalate-to-sulfate molar ratios in the two cloud categories (power plant plume in cloud and clouds uninfluenced by local pollution sources) show consistency and that the oxalate mass concentrations in cloud-free air were significantly lower is consistent with the hypothesis of an in-cloud production pathway for oxalate. Although SO_4^{2-} and oxalate are not directly linked chemically, the correlation between their levels is a result of the fact that both formation mechanisms require the aqueous medium. While information regarding the size distribution of oxalate and SO_4^{2-} is not available from the PILS measurements, past studies have noted similar size distributions of these two species, suggesting a common source [*Yao et al.*, 2003; *Crahan et al.*, 2004]. Further evidence for aqueous oxalate production is provided by the detection of aqueous intermediates in oxalate formation, including glyoxylate, which was measured in 6 CVI samples (clouds uninfluenced by local pollution sources) and 13 total aerosol samples (9 in clouds uninfluenced by local pollution sources and 4 in clouds influenced by power plant plumes).

4.2. Case Study: Power Plant Plume in Cloud (Flight 5 on 9 August 2004)

[19] On 9 August 2004 (1709–2216 UT), the TO sampled the Conesville Power Plant plume in cloud (Figure 5a). Located south of Cleveland, this plant emits SO_2 and NO_x at rates of 1.31×10^8 kg/yr and 2.16×10^7 kg/yr, respectively, and VOCs at 1.21×10^5 kg/yr (http://www.emissionsonline.org/nei99v3/plant/pl44374x.htm, 1999). The plume was transported northeast (~230°) at wind speeds between 6 and 12 m/s. Figure 5b shows the TO altitude, LWC, and aerosol number concentration. The TO flew a stair-step pattern between altitudes of 1500 and 2200 m downwind of the plant between 1815 and 2140 UT. LWC measurements reached values as high as 0.94 g/m^3.

[20] Typical FSSP cloud droplet size distributions showed a number concentration mode ranging from 7.7 to 9.0 μm with a geometric standard deviation ranging between 1.2 and 1.5. All instruments were sampling the total aerosol through the main inlet, which when used in cloud, as noted earlier, contained a mixture of interstitial aerosol, particles that contain significant amounts of water but are not activated (usually <2 μm), and droplet residuals. The DACAD measured a consistent bimodal size distribution with increasing distance downwind of the power plant in cloud, with a smaller mode that grew from 25 to 42 nm (Figure 6). The aerosol number concentration outside of cloud and close to the power plant was dominated by particles with D_p < 40 nm. A cloud-processing mode in the range between 100 and 200 nm was measured throughout the flight. The hygroscopic growth factor for the larger mode ranged between 1.16 and 1.20 at the relative humidities shown in Figure 6. The growth factors are low relative to that for pure ammonium sulfate particles (1.17 compared to 1.44 for pure ammonium sulfate at 77% RH), suggesting that the sampled aerosol was composed of less hygroscopic components.

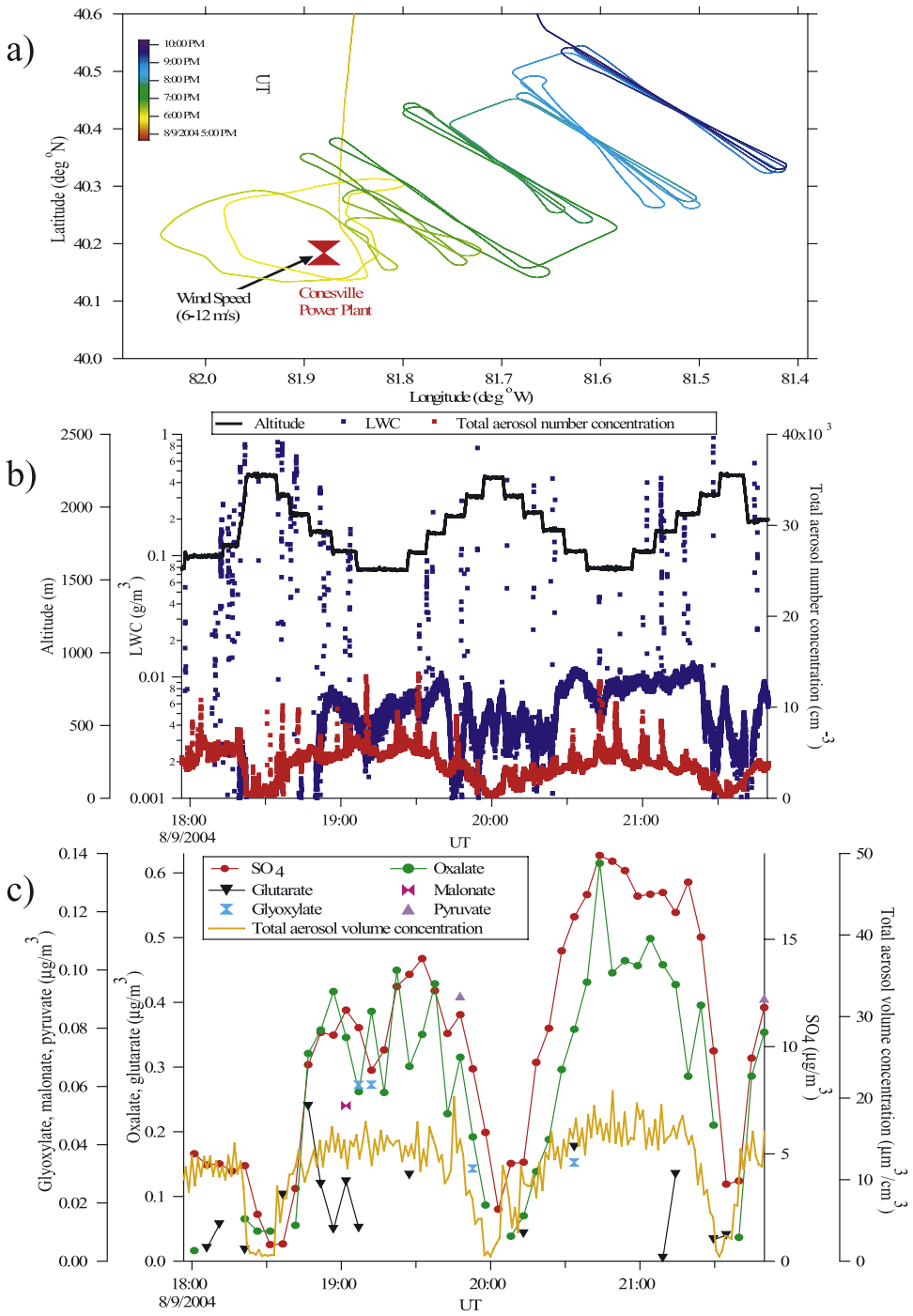

Figure 5. Flight 5 (9 August 2004): (a) flight tracks, (b) time series of altitude, LWC, and aerosol number concentration; and (c) time series of SO_4^{2-}, organic ions, and the aerosol volume concentration.

[21] Figure 5c shows a time series of SO_4^{2-}, various organic ions, and the volume concentration, from the DACAD, of the total aerosol sampled (D_p < 1 μm). There is significant growth in SO_4^{2-}, oxalate, and the aerosol volume concentration in the plume proceeding downwind of the power plant. The aerosol volume concentration and the SO_4^{2-} loadings are correlated and close in magnitude, suggesting that most of the volume growth was a result of the conversion of SO_2 to SO_4^{2-}. The ammonium-to-sulfate molar ratio was between 1.1 and 1.6 for most of the flight downwind of the plant, indicating that there was insufficient ammonia to neutralize the relatively high level of sulfuric acid. This high level of acidity can also explain why virtually no NO_3^- was detected (<0.3 μg/m^3). The aerosol volume concentration reached a maximum close to 40 km downwind of the plant (2043 UT), the point at which the highest SO_4^{2-} and oxalate loadings occurred (18.90 and 0.61 μg/m^3, respectively). Oxalate grew with increasing distance from the plant as well, representing between 0.5 and 3.1% of the total water-soluble mass for the majority of

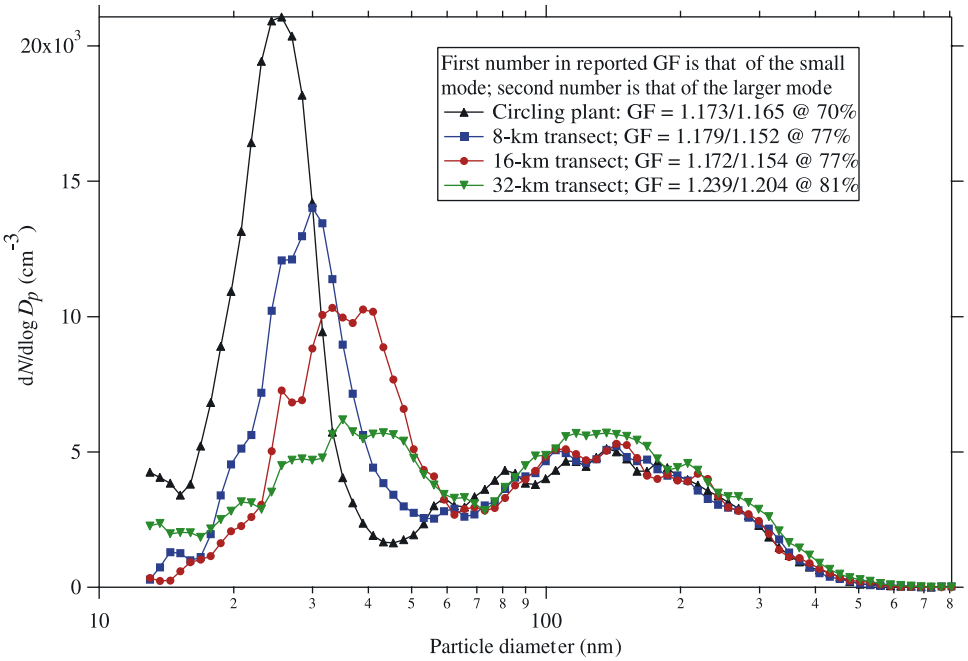

Figure 6. Evolution of the DACAD aerosol size distribution (dry: <20%) for flight 5 on 9 August 2004. GF refers to the aerosol growth factor at the RH value given.

the flight and 2.6% in the vial with its maximum mass. Out-of-plume, oxalate concentrations dropped below 0.1 μg/m^3, and SO_4^{2-} dropped to between 1 and 5 μg/m^3.

[22] Aqueous-phase precursors to oxalate were only identified in cloud, offering support to the hypothesis of an aqueous formation pathway. Glyoxylate, the anion of glyoxylic acid, was measured in two successive vials, at a level on the order of 0.06 μg/m^3, while oxalate was measured as 0.26 μg/m^3 and 0.39 μg/m^3 in these two vials. Two other vials contained 0.03 μg/m^3 glyoxylate, while oxalate was at 0.19 μg/m^3 and 0.36 μg/m^3. Pyruvate, the anion of pyruvic acid, which is thought to be a precursor of glyoxylic acid [*Lim et al.*, 2005], was measured at a level between 0.09 and 0.10 μg/m^3. Glutarate, the anion of the glutaric acid (C_5 dicarboxylic acid), reached a maximum level of 0.24 μg/m^3. One vial contained 0.05 μg/m^3 of malonate, the anion of malonic acid (C_3 dicarboxylic acid). Longer-chain dicarboxylic acids such as glutaric acid are oxidized in the aqueous phase leading to smaller dicarboxylic acids, ultimately reaching oxalic acid [*Kawamura and Sakaguchi*, 1999]. The aforementioned data alone do not reveal the relative contribution from the decay of longer-chain acids such as glutarate and the oxidation of glyoxylate to the production of oxalate mass; this will be explored subsequently.

[23] Since the concentrations of SO_4^{2-} and oxalate are correlated and they are both typically found in the same mode in the submicrometer aerosol size range, it is hypothesized that oxalate is formed in the aqueous phase, for which the presence of key aqueous intermediates to oxalic acid provides evidence. The mass concentrations of SO_4^{2-} and oxalate were higher in the flight 5 total aerosol samples as compared to the total aerosol and droplet residual measurements in clouds uninfluenced by local pollution sources from other flights. This is hypothesized to be a result of longer cloud processing times for sampled particles during flight 5 since the clouds were more abundant and closely packed. Also, some of the highest LWC values from the entire mission were observed, leading to increased partitioning of gases (specifically SO_2, organic precursors to oxalic acid, and oxidants) into the droplets, yielding higher mass production rates of SO_4^{2-} and oxalate. The highly turbulent nature of the lower atmosphere on 9 August 2004 may have also promoted the reactivation of evaporated droplets, via cycling in and out-of-cloud, to produce increasing amounts of SO_4^{2-} and oxalate. We note that although the SO_2 concentrations were measured to be higher in plume compared to nonplume conditions, the concentrations of volatile organic carbon (VOC) species were essentially similar, which highlights the importance of non-VOC factors in oxalic acid production.

5. Cloud Parcel Model

5.1. Description and Modifications

[24] The overall goal of this study is to understand the mechanism of occurrence of oxalic acid in atmospheric aerosols. The hypothesis is that aqueous-phase chemistry provides the dominant route for oxalic acid formation. To evaluate the extent to which the data support this hypothesis, we compare ambient oxalate measurements to predictions of a state-of-the-art microphysical/chemical cloud parcel model [*Ervens et al.*, 2004] that simulates the activation of a population of aerosol particles. The model also simulates cloud cycles that are intended to represent the trajectory of a typical air parcel in a cloudy atmosphere, including gas and aqueous-phase chemical reactions. Four gas-phase VOC precursors of dicarboxylic acids are included; toluene and ethene represent anthropogenic emissions, isoprene represents biogenic emissions, and

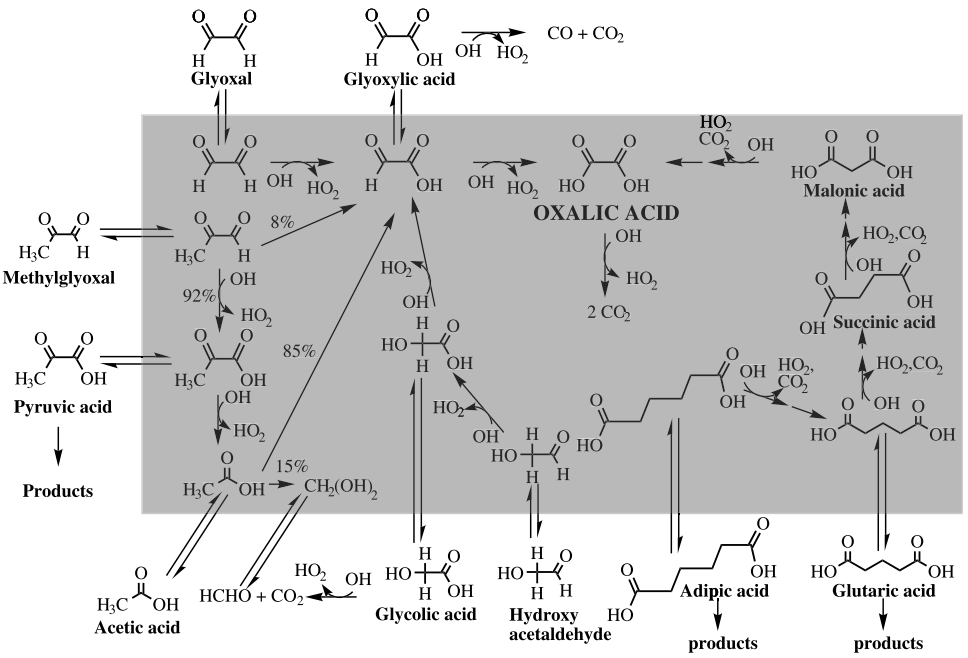

Figure 7. Multiphase organic chemistry (shaded area indicates aqueous phase). References are *Ervens et al.* [2004] and *Lim et al.* [2005].

cyclohexene serves as a model compound for symmetrical alkenes similar to monoterpenes emitted by biogenic sources. The oxidation products of these species in the gas phase (glyoxal, glyoxylic acid, glycolic acid, hydroxyacetaldehyde, methylglyoxal, pyruvic acid, acetic acid, adipic acid, and glutaric acid) can transfer to the aqueous phase. Key multiphase organic reactions leading to the formation and depletion of oxalic acid are shown in Figure 7, whereas SO_4^{2-} production in the model is simply governed by SO_2 oxidation with H_2O_2 and O_3 [*Seinfeld and Pandis*, 1998]. The model does not consider the volatilization of particulate dicarboxylic acids as their vapor pressures are sufficiently low ($<10^{-5}$ mm Hg) [*Saxena and Hildemann*, 1996; *Tong et al.*, 2004].

[25] Oxalic acid has two sources and one sink in the aqueous phase; it is consumed by OH oxidation to yield CO_2, and it is formed by OH oxidation of longer-chain dicarboxylic acids and glyoxylic acid (including its anion, glyoxylate). The formation route arising from the decay of longer dicarboxylic acids begins with adipic acid, which is formed primarily by the aqueous uptake of gas-phase products from cyclohexene oxidation by ozone and OH. Glutaric acid is formed by the aqueous oxidation of adipic acid and by the aqueous uptake of gas-phase products from the ozonolysis of cyclohexene. A series of oxidation steps leads, in order, from glutaric acid to succinic, malonic, and oxalic acids. The second formation route considers the oxidation of glyoxylic acid, which is formed by the OH oxidation of glyoxal, glycolate, methylglyoxal, and acetic acid. These intermediates are formed in the mechanisms associated with toluene, isoprene, and ethene. *Lim et al.* [2005] have proposed that methylglyoxal yields low volatility organic acids through oxidation to glyoxylic acid, via intermediate steps involving pyruvic and acetic acids, and finally to oxalic acid. The *Ervens et al.* [2004] aqueous-phase mechanism for isoprene oxidation has been modified to account for these reactions (Figure 7).

[26] The model was applied to match the conditions encountered in the ICARTT flights. To estimate the soluble aerosol fraction (by mass), the total PILS water-soluble mass (inorganic and organic acid species) was divided by the sum of the PILS inorganic water-soluble mass and the organic mass measured by the AMS. The AMS organic measurement includes both water-soluble and nonwater soluble species. The model was also modified to incorporate measured ambient particle size distributions.

[27] Since measurements were carried out in plumes, it is necessary to account for plume dispersion. Using measurements and estimates for various properties in the background air (including concentrations of SO_2, H_2O_2, O_3, gas-phase organic precursors, and the mixing ratio of water), the following parameterized factor, which will be called the entrainment rate, is applied to simultaneously simulate open system conditions and plume dilution,

$$\frac{\partial \phi_c}{\partial t} = -\frac{\eta}{b}(\phi_c - \phi_e)$$

where ϕ_c and ϕ_e are the values of a property in the moving parcels and in the entrained air, respectively. As will be discussed later, a constant measured value representative of background air in the ambient Ohio atmosphere was used for properties represented by ϕ_e, while ϕ_c was initialized with measured values at the source of the ambient process being simulated (one simulation to be addressed in a later section begins near a power plant stack) and subsequently calculated after each time step by the model. The equation above is analogous to the plume entrainment rate presented by *Squires and Turner* [1962], where a value of $\eta = 0.2$ is based on their laboratory experiments. The parameter b is

defined as the characteristic length scale for the entrainment process at time t, and taken here as 500 m, the typical depth of the clouds sampled. It is emphasized that the entrainment rate represents a simplified ad hoc factor.

[28] The model simulates 1-hour cloud cycles that are intended to represent the trajectory of a typical air parcel in a cloudy atmosphere. Twelve cloud cycles, limited by the prescribed trajectory used, are simulated for each experiment. One cloud cycle begins with a parcel of air ascending from near the ground up through the mixed layer until activation in cloud. The parcel continues to rise and then descends through the cloud back to the mixed layer. During each cycle, a parcel is in-cloud for approximately 800 s; the same trajectory is then repeated with the number concentration remaining the same, but with particle sizes altered because of mass addition after each cycle. The LWC time evolution in the prescribed thermodynamic trajectory represents mixing and drying by entrained air, based on the host model from which it is derived. A rough estimate of the in-cloud residence time can be estimated by calculating the volume fraction of the boundary layer (BL) occupied by cloud [*Feingold et al.*, 1998]; typical volume fractions observed were between 20 and 25% suggesting that the hourly cloud contact time was between 720 and 900 s for a well-mixed BL, a range that is consistent with the cloud contact time of 800 s assumed in the cloud cycles. Photolysis rates are calculated for 40°N on 21 June at a height of 1 km for 12 hours starting at 6 am. The photolysis rates are time-dependent and uninfluenced by the presence of clouds. Gas uptake and chemical aqueous-phase processes during each cycle occur only if the LWC exceeds 1 mg/kg and for each particle size bin if the sum of the ammonium and sulfate concentrations does not exceed 1 M. The model neglects aqueous-phase chemical processes when the ionic strength exceeds 1 M. This assumption is the result of a lack of data for the estimation of rate coefficients and because the solubility of organic gases typically decreases with increasing ionic strength. The model also does not consider aerosol loss by wet and dry deposition. Predictions for SO_4^{2-} and oxalate levels are presented here at the end of each cloud cycle. The comparison between field data and predictions should be viewed as semiquantitative; for instance, the actual trajectories of air parcels are not known. Our goal is to determine the extent to which the levels of SO_4^{2-} and oxalate measured are generally consistent with those predicted by a model that is based on cloud processing and aqueous-phase chemistry.

5.2. Sensitivity Analysis

[29] Prior to actually simulating the field data, we explore the sensitivity of the model to key parameters and initial conditions related to the initial particle population and the ambient atmosphere which include meteorological conditions and concentrations of gaseous species. *Ervens et al.* [2004] simulated generic "clean continental" and "polluted" cases, in which for a closed system (without entrainment of background air) SO_4^{2-} reached its ultimate level by the end of the third cloud cycle. With continuous replenishment of SO_2, on the other hand, SO_4^{2-} is predicted to form continuously. Oxidation of all organic species in the aqueous phase yields HO_2 which replenishes the H_2O_2 supply, also promoting SO_4^{2-} production. Sulfate production is controlled mainly by the initial concentrations of SO_2 and H_2O_2; a set of simulations show that the percentage change in SO_4^{2-} mass depends almost linearly on the percentage change in the initial SO_2 concentration, while an increase in H_2O_2 yields a less than proportional increase in SO_4^{2-}. The initial value of SO_4^{2-} is governed by the size distribution and soluble fraction of the initial particle population, where the initial soluble portion is assumed to be pure ammonium sulfate.

[30] *Ervens et al.* [2004] showed that approximately eight cloud cycles are required for aqueous-phase organic oxidation to be completed in "clean continental" and "polluted" cases (since organics are involved in more oxidation steps than SO_4^{2-}). As with sulfur, with continued replenishment of organic precursor gases, organics continue reacting in the aqueous phase. Oxalic acid production does not exhibit the same degree of sensitivity to its precursor concentrations as does SO_4^{2-} to SO_2. In some cases, even less oxalic acid was produced when its gaseous precursor concentrations were increased. One explanation is that oxalic acid does not form in direct proportion to its parent precursor VOC (toluene, ethene, isoprene, cyclohexene) levels because of subsequent steps required in its formation and competing reactions that deplete OH, the primary oxidant in the aqueous-phase organic reactions. Examples of such competing reactions include the OH oxidation of hydrogen peroxide, formic acid, formate, and hydrated formaldehyde. In addition, several volatile organic species, including HCHO and CO_2, are produced as side-products in the aqueous-phase mechanism and do not contribute to oxalic acid production.

[31] The base value of 500 m used for b in the entrainment rate was doubled and halved to explore the sensitivity of the production rates of SO_4^{2-} and oxalic acid to this parameterized factor. For these sensitivity tests, the concentrations of gas-phase species in the moving parcels (ϕ_c) and in the entrained air (ϕ_e) were identical and equal to the initial conditions for the case of clouds uninfluenced by local pollution sources in Table 4. As will be discussed later, these conditions are taken from field measurements made at 1000 m in the ambient Ohio atmosphere. With higher entrainment rates, the simulated particles are more effectively replenished with oxidants, SO_2, and organic precursors. Sulfate steadily changed to reach a final mass 28.3% greater and 27.2% lower when the entrainment rate was doubled and halved, respectively. Doubling and halving the base entrainment rate yielded 11% more and 3% less oxalic acid, respectively, at the end of the simulation. Although less oxalic acid was formed in the case with the lowest replenishment rate of oxidants and precursors, oxalic acid was produced more efficiently relative to the total organic mass compared to simulations with higher entrainment rates; the oxalic acid predicted contribution to the total organic aerosol mass in the case with the lowest entrainment rate exceeded that of the other two cases by a minimum of 40% after the second cloud cycle. Concentrations of the first-generation aqueous-phase organic products, like adipic acid, showed the most proportional response to changes in the entrainment rate (they grew with increasing entrainment rate) followed by-products in subsequent generations. Thus the nonlinear response of oxalic acid to the entrainment rate compared to SO_4^{2-} can be explained by the multiple steps required in oxalic acid formation and the complex feedbacks of reaction chains in the chemical mechanism, spe-

Table 4. Initial Conditions for Two Simulations[a]

	Power Plant Plume in Cloud, ppb Unless Otherwise Stated	Clouds Uninfluenced by Local Pollution Sources, ppb Unless Otherwise Stated
SO_2	69.5	0.5
O_3	40.0	40.0
H_2O_2	1.0	1.0
NH_3	0.25	0.25
HNO_3	2.0	2.0
CO_2	360 ppm	360 ppm
N_2O_5	0.02	0.02
HCHO	1.5	1.5
CH_2OHCHO	1.0	1.0
$(CHO)_2$	1.0	1
$CH_3C(O)CHO$	1.0	1.0
HCOOH	0.5	0.5
CH_3COOH	1.0	1.0
CH_3CHO	1.0	1.0
$CH_3C(O)CH_3$	1.0	1.0
$C_6H_5CH_3$ (toluene)	0.11	0.06
C_2H_4 (ethene)	0.13	0.05
C_6H_{10} (cyclohexene)	0.01	0.01
C_5H_8 (isoprene)	0.04	0.04
NO	3.27	0.07
NO_2	9.42	0.50
CO	118.0	114.1
CH_4	1842.0	1825.0

Initial D_p, nm	Power Plant Plume in Cloud: N, cm^{-3} (Sum = 4890 cm^{-3})	Clouds Uninfluenced by Local Pollution Sources: N, cm^{-3} (Sum = 1755 cm^{-3})
828.2	20	0
574.4	2.34	0.435
340.6	88	9.8
212.8	471	52.3
140.1	711	146.6
113.6	502	90.7
97.2	549	129.6
51.9	1219	486
36.0	343	351
17.3	767	489
9.7	238	0.426

	Power Plant Plume in Cloud	Clouds Uninfluenced by Local Pollution Sources
Soluble fraction by mass, %	45	60
T, C	15	15
P, bar	900	900
Altitude, m	1000	1000
RH, %	70	70

[a]Conditions for clouds uninfluenced by local pollution sources are also those representing the background air in the entrainment rate for both simulations.

cifically with the oxidant cycles (including HO_x, NO_x, O_3, and H_2O_2). Also, the production of oxalic acid from glyoxylic acid oxidation is less efficient as the pH decreases, with the lowest pH values predicted in the simulation with the highest entrainment rate, because the rate constant of the oxidation of glyoxylic acid is an order of magnitude lower than that of its anion, glyoxylate.

[32] The results of these sensitivity tests emphasize the critical nature of allowing for an open system with entrainment as opposed to a closed system when simulating the production rates of SO_4^{2-} and oxalic acid. Sulfate was shown to be the most sensitive to its precursor concentrations (SO_2). Although the total organic aerosol mass and SO_4^{2-} are comparably sensitive to their precursor concentrations, oxalic acid is not. This is because the total organic mass is dominated by first-generation products in the aqueous phase, mainly adipic acid. Several oxidation steps are required to form oxalic acid, which allows for the depletion of OH, the primary oxidant for organic compounds, and the production of volatile organic side-products that do not contribute to the production of oxalic acid.

6. Comparison of Model Predictions to Field Measurements

[33] Measured ambient conditions from two specific flights (Table 4) are used here to initialize individual simulations to represent the two types of clouds that were studied; flights 5 (9 August 2004) and 12 (21 August 2004) represent power plant plume in cloud and clouds uninfluenced by local pollution sources, respectively. The representative measurements from flight 5 were made directly downwind of the Conesville Power Plant outside of cloud in its plume at 1000 m, whereas the flight 12 measurements were made at the same altitude at a location in the Ohio atmosphere unaffected by local pollution sources. Gas-phase measurements were not carried out on the TO; estimates of the gaseous precursor concentrations were obtained from the WP-3D and Convair, operated by NOAA and the Meteorological Service of Canada (MSC), respectively, which flew in the same areas as the TO, but at different times. In both simulations, concentrations of gas-phase species in the entrained air were set equal to those in the case of clouds uninfluenced by local pollution sources (Table 4), which represent background air conditions. Two key differences in the plume case are the higher SO_2 and aerosol number concentrations. Although the ethene and toluene levels are each below 0.15 ppb for both cases, they are nearly twice as large in the plume case suggesting that anthropogenic emissions were stronger directly downwind of the Conesville plant compared to a nearby location in the Ohio atmosphere unaffected by local pollution sources. The soluble fraction of the initial particle population in the plume case is calculated to be 0.45 as opposed to 0.60 for clouds uninfluenced by local pollution sources. These two values agree with an alternate calculation of the soluble fraction by dividing the total PILS water-soluble mass by the DACAD-derived mass concentration assuming a total aerosol density of 1.3 g/cm^3 in both cases. Measurements show that the sampled particles from the plume flight were composed of less hygroscopic components; the accumulation mode (100 to 200 nm) growth factors for the representative measurements during flight 5 and 12 were 1.15 (77% RH) and 1.20 (75% RH), respectively. For the aerosol microphysics, it is assumed that the soluble fraction is entirely ammonium sulfate. The measured contribution of ammonium and sulfate to the total water-soluble mass measured by the PILS was on the order of 90% for the representative data for both flights; thus the predicted SO_4^{2-} concentrations are adjusted accounting for the 10% deficit in the initial water-soluble ammonium sulfate mass.

6.1. Case Study: Power Plant Plume in Cloud

[34] Figure 8 shows predictions for the growth rate of SO_4^{2-} and various organic ions in the particle phase imme-

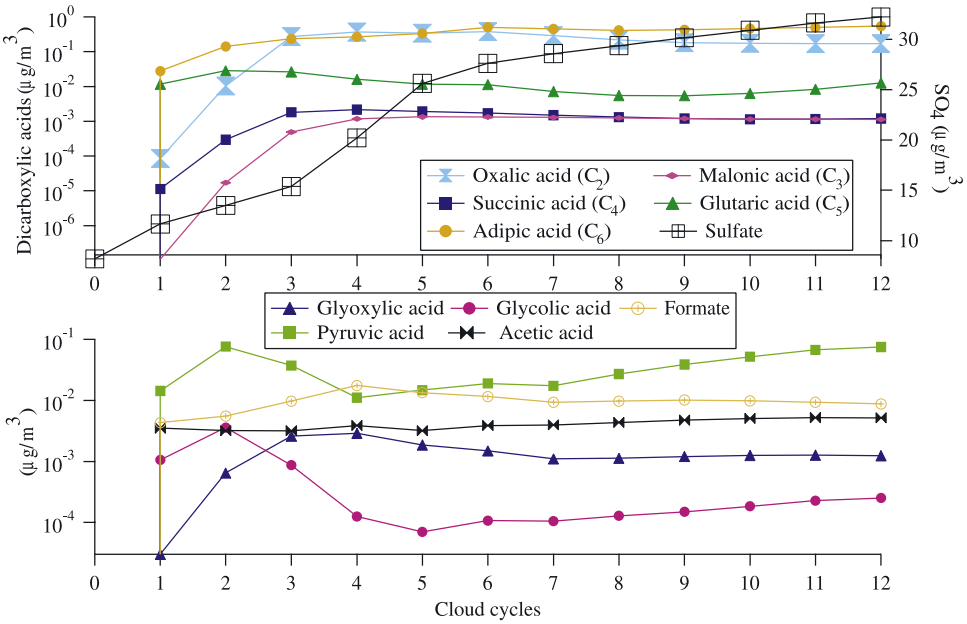

Figure 8. Model predictions for the power plant plume in cloud case (simulation of flight 5 on 9 August 2004).

diately downwind of the Conesville Power Plant. Sulfate is predicted to continuously increase, reaching a total submicrometer mass of 31.4 μg/m^3, with its sharpest increase predicted during cloud cycles 4 and 5. The predicted total organic mass, which grows to 0.82 μg/m^3 by the end of the simulation, is dominated by oxalic and adipic acids (the model treats the oxidation of cyclohexene as a one-step process leading immediately to adipic acid). *Ervens et al.* [2004] state that the cyclohexene mechanism provides an upper estimate for its contribution to the predicted dicarboxylic acid mass due to the simplified (one-step) chemistry in the model. The background concentration of cyclohexene is assumed to be 0.01 ppb, which was chosen to stay consistent with previous measurements showing that its emission rate is an order of magnitude less than that of toluene [*Grosjean and Fung*, 1984]. Even though the background concentration of cyclohexene, which was not measured by the WP-3D or Convair, in the atmosphere above Ohio may have been lower since adipate was not measured by the PILS, cyclohexene can be considered to serve as a surrogate compound for all symmetrical alkenes similar to monoterpenes.

[35] Adipic and glutaric acids are oxidized, forming the shorter-chain acids starting with succinic acid, which then fuels malonic acid production. Succinic and malonic acids are each predicted to remain below 0.01 μg/m^3 and 0.3% of the total organic mass throughout the simulation. The oxidation of malonic acid leads to oxalic acid, which is predicted to grow to levels comparable to those of adipic acid (0.27 μg/m^3 and 0.24 μg/m^3, respectively) after three cloud cycles since it is also produced by glyoxylic acid oxidation. Oxalic acid reaches a peak mass of 0.38 μg/m^3 after the sixth cloud cycle before steadily decreasing to 0.17 μg/m^3 by the end of the simulation. It grows the most during the third and fourth cloud cycles, which corresponds to the two cycles with the highest average droplet pH values (2.61 and 2.46, respectively) and when glyoxylic acid and its precursors reached their highest concentrations (droplet pH values from the simulations will be displayed subsequently).

[36] Figure 9 compares predictions to field measurements from flight 5, where first-order plume age is based on the distance away from the power plant and the wind speed. Selected measurements from the field data were taken to represent different distances downwind of the Conesville Power Plant where transects were made. The field measurements for SO_4^{2-} show continuous growth until the last transect where plume dilution may have dominated. The initial SO_4^{2-} mass predicted prior to the first cloud cycle (cloud cycle 0 in Figure 9) is highly dependent on the assumed particle size distribution and soluble fraction of the particles used to initialize the simulation. Using the measured values for these two parameters, the initial SO_4^{2-} predicted (7.37 μg/m^3) is already more than 2 μg/m^3 greater than that measured in the first transect downwind of the Conesville Power Plant (5.00 μg/m^3 at a plume age of 0.6 hours). The model predicted that 3.46 μg/m^3 of SO_4^{2-} grew after the first cloud cycle, while the most growth occurs in the fourth and fifth cloud cycles (4.83 μg/m^3 and 5.42 μg/m^3, respectively). Sulfate grows between 0.5 and 2 μg/m^3 in each of the other cloud cycles. It is hypothesized that SO_4^{2-} increased the most during cloud cycles 4 and 5 because the average cloud cycle droplet pH value experienced its largest decline in the simulation from 2.61 in the third cycle to 1.95 in the fifth cycle, which enhanced SO_4^{2-} production.

[37] Oxalic acid first increases and eventually decreases slightly with downwind distance in both the field data and the predictions. The decrease in oxalic acid is predicted to be due to its oxidation in the particle phase to CO_2. The predicted oxalate-to-sulfate molar ratio agrees with the field data points (between 0.01 and 0.05) from the third cloud cycle until the end of the eighth cloud cycle.

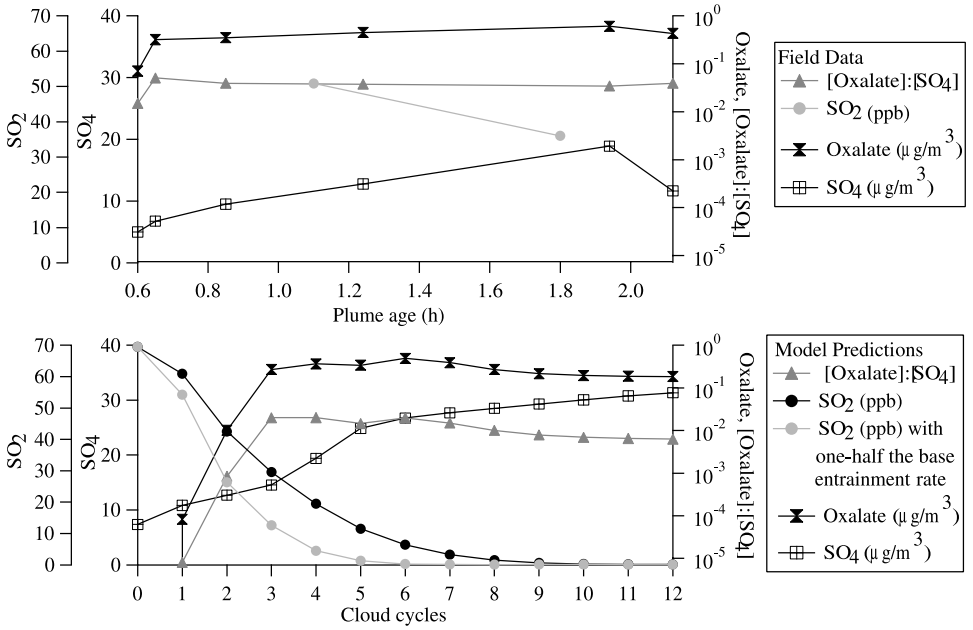

Figure 9. Comparison of flight 5 (9 August 2004) field data and model predictions for SO_4^{2-} and oxalate growth.

[38] As mentioned earlier, it is difficult to compare plume age, as measured by the aircraft, to a specific cloud cycle, as represented by the model. A tracer species such as SO_2 can give an indication of the comparison of field data at different transects to predictions from specific cloud cycles. The NOAA WP-3D made measurements of SO_2 on 6 August 2004 in the Conesville plume at distances corresponding to plume ages of 1.1 hours (51 ppb) and 1.8 hours (36 ppb), which occur during the second cloud cycle. Figure 9 shows how the predicted SO_2 concentration changes at one half the base entrainment rate. At this lower rate, the second measured point for SO_2 is predicted to occur during the third cloud cycle. The oxalate measurement between plume ages of 1.1 and 1.8 hours (0.45 $\mu g/m^3$) substantially exceeds predictions between the first and second cloud cycles (9×10^{-5}–0.01 $\mu g/m^3$); it does, however, agree within an order of a magnitude with the predictions starting from the third cloud cycle until the last cycle, ranging between 0.17 and 0.38 $\mu g/m^3$. The ambient SO_4^{2-} measurement (12.8 $\mu g/m^3$) lies between the values predicted between the second and third cloud cycles (12.68–14.55 $\mu g/m^3$). Thus measurements and predictions for the relative levels of SO_4^{2-} and oxalate agree to within one cloud cycle when considering the same amount of SO_2 measured and predicted.

[39] The measured glyoxylate concentrations during flight 5 ranged between 0.03 and 0.06 $\mu g/m^3$ (Figure 5c), which exceed the predicted values by an order of magnitude. The model predicted up to 0.08 $\mu g/m^3$ of pyruvic acid, which is close to that observed flight 5 (0.09–0.10 $\mu g/m^3$). Glutaric acid, measured at levels between 0.02 and 0.24 $\mu g/m^3$ during flight 5, is predicted to reach a peak of 0.03 $\mu g/m^3$ after the second cloud cycle. Malonic acid (0.05 $\mu g/m^3$) was measured as an order of magnitude larger than predictions, which were stable after the fourth cloud cycle at 0.001 $\mu g/m^3$. In summary, measured and predicted mass concentrations of organic acids other than oxalic acid in the particle phase show general agreement, providing support for the aqueous-phase chemical mechanism used to predict oxalic acid formation.

6.2. Case Study: Clouds Uninfluenced by Local Pollution Sources

[40] Figure 10 shows predictions from a simulation initialized with conditions representative of the absence of local pollution sources, including power plant plumes. Sulfate is predicted to grow almost linearly with each successive cloud cycle from 1.4 to 12.5 $\mu g/m^3$. The total organic mass, which is predicted to grow to 3.06 $\mu g/m^3$ at the end of the simulation, once again has its largest dicarboxylic acid mass contributions from oxalic and adipic acids. Oxalic acid is predicted to achieve its peak concentration after the fourth cloud cycle (0.61 $\mu g/m^3$), which corresponds to the cycle with the highest average droplet pH value (3.28), before steadily decreasing to 0.35 $\mu g/m^3$ at the end of the simulation. Glyoxylic acid is predicted to increase in concentration with each successive cloud cycle, in contrast to its behavior in the power plant plume in cloud case. Glyoxylic acid is also predicted to attain higher concentrations in this case as compared to the previous case study (0.2 $\mu g/m^3$ versus 0.002 $\mu g/m^3$). The concentrations of the precursors to glyoxylic acid (including acetic, pyruvic, and glycolic acids) are also predicted to be greater in this case, suggesting that the mechanisms associated with toluene, ethene, and isoprene (only these three parent organic species produce glyoxylic acid) are more efficient at producing oxalic acid. The pathway associated with cyclohexene, which consists of the decay of dicarboxylic acids (from C_6 to C_2) by OH oxidation and does not involve any other aqueous-phase intermediate species, is more efficient in the previous case at producing oxalic acid since a greater amount of the C_3-C_6 acids were produced.

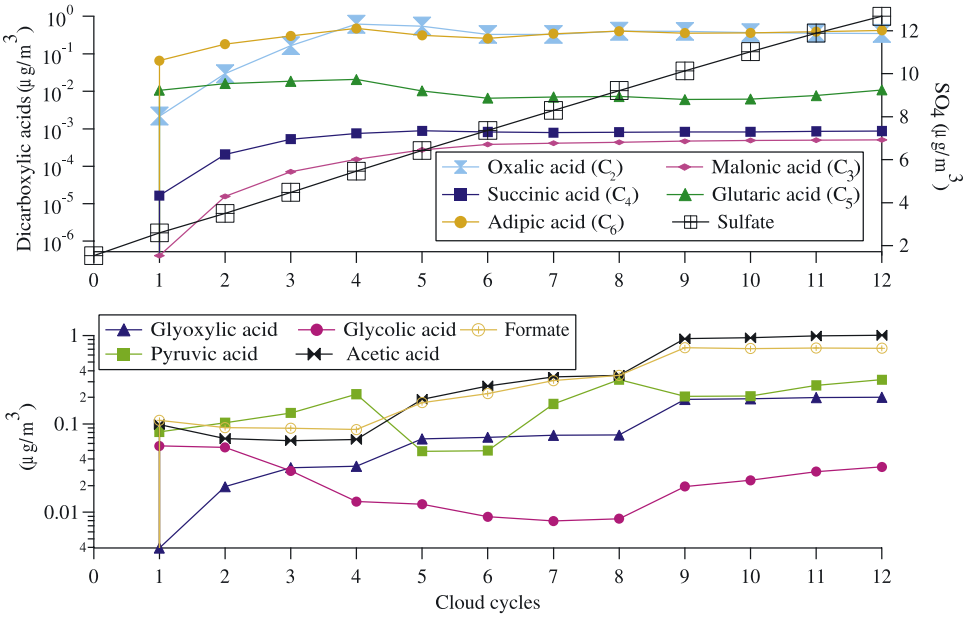

Figure 10. Model predictions for the case of clouds uninfluenced by local pollution sources.

[41] That more oxalic acid is predicted to form in this case as compared to that of the power plant plume in cloud case is a result of the predicted relative effectiveness of glyoxylic acid oxidation versus the decay of longer-chain dicarboxylic acids. The production of glyoxylic acid was less efficient in the previous simulation due partly to the lower soluble fraction of the initial particle population (0.45 versus 0.60 for plume and nonplume cases, respectively). The partitioning of gas-phase species into droplets was reduced in the plume simulation since the LWC was lower. Also, the effective Henry's Law coefficients are a function of pH; the more acidic particles in the plume simulation (total simulation pH average of 1.88 versus 2.46 for plume and nonplume cases, respectively) resulted in a reduction of the droplets' uptake efficiency for some aqueous-phase precursors to oxalic acid, including acetic and pyruvic acids. As stated before, although sulfate production is enhanced at lower pH, the production of oxalic acid from glyoxylic acid is slower at lower pH because the rate constant of the oxidation of glyoxylic acid is an order of magnitude lower than that of its anion, glyoxylate.

6.3. Comparison of Predictions From Both Cases to All In-Cloud Field Measurements

[42] Figure 11 compares all of the measured oxalate and SO_4^{2-} data from total aerosol and droplet residual samples to the predictions of the two previous case studies. Predictions of the relative growth of SO_4^{2-} versus oxalate from the first three cloud cycles, corresponding to up to 40 min of cloud contact time, agree most closely with ambient measurements for clouds uninfluenced by local pollution sources. The high droplet pH values during the fourth and fifth cloud cycles yielded greater predicted oxalate growth relative to SO_4^{2-} compared to observations; however, the relative amounts of the two species are again predicted to come close to agreement with observations after the fifth cycle. Predictions during the third and fourth cloud cycles (between 40 and 55 min of cloud contact time) agree with the power plant plume in cloud measurements. Cumulatively, for both cloud types studied, the relative loadings of SO_4^{2-} and oxalate predicted during the third cloud cycle agree the best with observations, suggesting that the average air parcel experienced nearly 40 min of cloud contact time. In addition, the ranges of SO_4^{2-} and oxalate measured agree with those predicted for both cloud types, with the exception of the large amount of SO_4^{2-} predicted after the fourth cloud cycle for the case of power plant plume in cloud.

[43] As noted earlier, the measured amounts of oxalate relative to SO_4^{2-} downwind of the Conesville plant exceeded those predicted, indicating that the model overestimated SO_4^{2-} production relative to oxalate in the case of power plant plume in cloud. If the aerosol number concentration or the soluble fraction used to initialize the particle population in the power plant plume in cloud simulation were slightly lower, the SO_4^{2-} levels would be reduced to a greater extent compared to oxalate, yielding better agreement between measurements and predictions. Even though these two values were derived from measurements, any error in the determination of these initial values could have led to inaccurate predicted SO_4^{2-} levels. Also, the overestimate in SO_4^{2-} may be due to the actual plume dilution in flight 5 being higher than assumed. Excess SO_4^{2-} and oxalate predicted in the latter cloud cycles for clouds uninfluenced by local pollution sources may have resulted from a replenishment rate of oxidants, organic precursors, and SO_2 that is too high. However, the latter cloud cycles that predicted excessive SO_4^{2-} and oxalate in both simulations may also represent particles that were processed longer compared to the sampled particles.

[44] The model predicts a range of particulate oxalic acid levels that are consistent with measurements of both total aerosol and droplet residuals in clouds. The predicted growth of oxalate relative to SO_4^{2-} is most consistent with measurements assuming that the sampled particles experienced an average of 40 min of cloud contact time. However, if the sampled particles had been processed longer, the

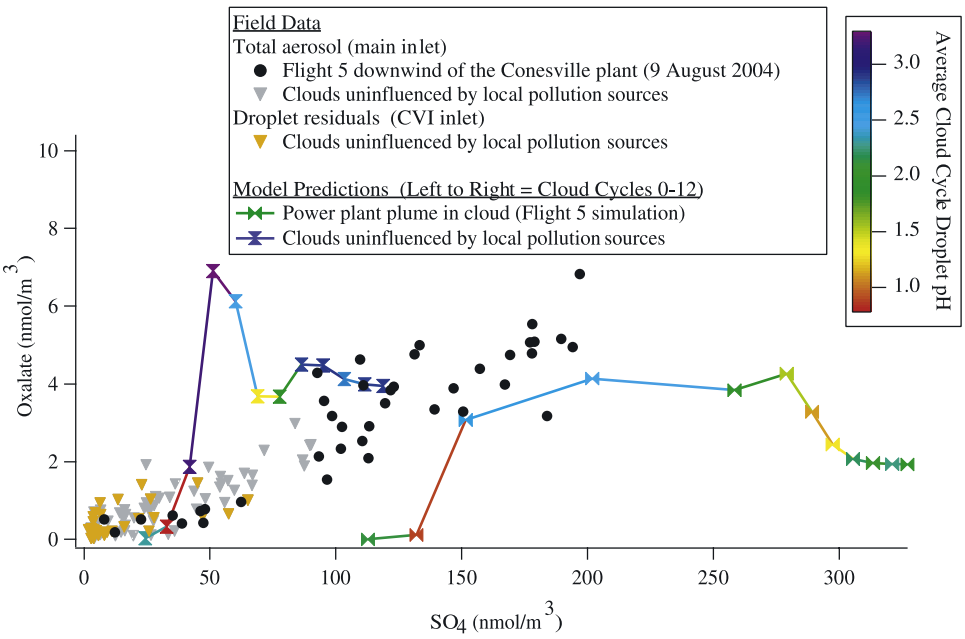

Figure 11. Comparison of oxalate and SO_4^{2-} molar concentrations between model predictions and field data for clouds with and without power plant plume influence. The model prediction points are color coded to represent the average droplet pH during each cloud cycle.

predicted replenishment of gaseous species in the entrained air may have been too high, leading to an overestimate in the latter cloud cycles for SO_4^{2-} (both simulations) and oxalate (only in the case of clouds uninfluenced by local pollution sources). Also, uncertainties in the characteristics of the initial particle population may have led to inaccurate predicted SO_4^{2-} growth relative to oxalate.

6.4. Contribution of Different Aqueous-Phase Pathways to Production of Oxalic Acid

[45] Comparison of observations and predictions can help address the relative importance of different aqueous-phase oxalic acid formation pathways. Three simulations were performed, using the conditions from the case of clouds uninfluenced by local pollution sources in Table 4 (the initial concentration of cyclohexene was set to 0.05 ppb instead of 0.01 ppb to compare the predicted oxalic acid growth to the simulation presented in section 6.2), to analyze the effect of the two pathways, decay of larger dicarboxylic acids versus oxidation of glyoxylic acid. In the first case, only cyclohexene was considered as an organic precursor; in this case, oxalic acid is produced only from the decay of longer-chain dicarboxylic acids. The second case considered toluene, isoprene, and ethene as organic precursors in the absence of cyclohexene; this case assesses oxalic acid formation solely from the oxidation of glyoxylic acid. The third simulation, which is that presented for the case of clouds uninfluenced by local pollution sources, included all four of the organic precursors.

[46] Figure 12 shows the evolution of oxalic acid in all three simulations. The cyclohexene-only simulation predicts a peak in oxalic acid concentration after the sixth cloud cycle of 0.0008 $\mu g/m^3$. The simulation with the other three organic precursors predicts a maximum of oxalic acid after the fourth cloud cycle of 0.64 $\mu g/m^3$. The simulation with all four organic precursors leads to an oxalic acid peak after the fifth cloud cycle of 0.57 $\mu g/m^3$. These results show clearly that the oxidation of glyoxylic acid dominates the aqueous-phase production of oxalic acid. The predicted levels of malonic, succinic, glutaric, and adipic acids from the cumulative case and that considering only cyclohexene are nearly identical, but the difference in predicted oxalic acid levels is significant. The oxalic acid levels predicted in the case considering all the organic precursors nearly matches that in the absence of cyclohexene, demonstrating the dependence of oxalic acid formation on the oxidation of glyoxylic acid. The key difference after increasing the initial cyclohexene concentration from 0.01 to 0.05 ppb was a near five-fold increase in the production of glutaric and adipic acids. As explained above, these two species do not contribute significantly to oxalic acid production making little difference in the oxalic acid concentrations during the simulation.

7. Conclusions

[47] Airborne measurements made during ICARTT 2004 in the vicinity of Ohio provide clear evidence for aqueous-phase production of oxalic acid. In addition, a correlation between measured oxalate and SO_4^{2-} is indicative of common aqueous-phase processing, as these two species are not directly linked in their production chemistry. The highest mass loadings for oxalate were measured for total aerosol and droplet residual samples in clouds influenced by power plant plumes. Virtually no oxalate was measured in cloud-free air aerosols; however, values slightly higher than detection limits were observed for aerosol samples in a power plant plume in cloud-free air. The strongest correlation between SO_4^{2-} and oxalate ($R^2 = 0.80$, $n = 40$) is seen in flight 5 (9 August 2004) where the aircraft was sampling the total aerosol downwind of a coal-fired power plant in the

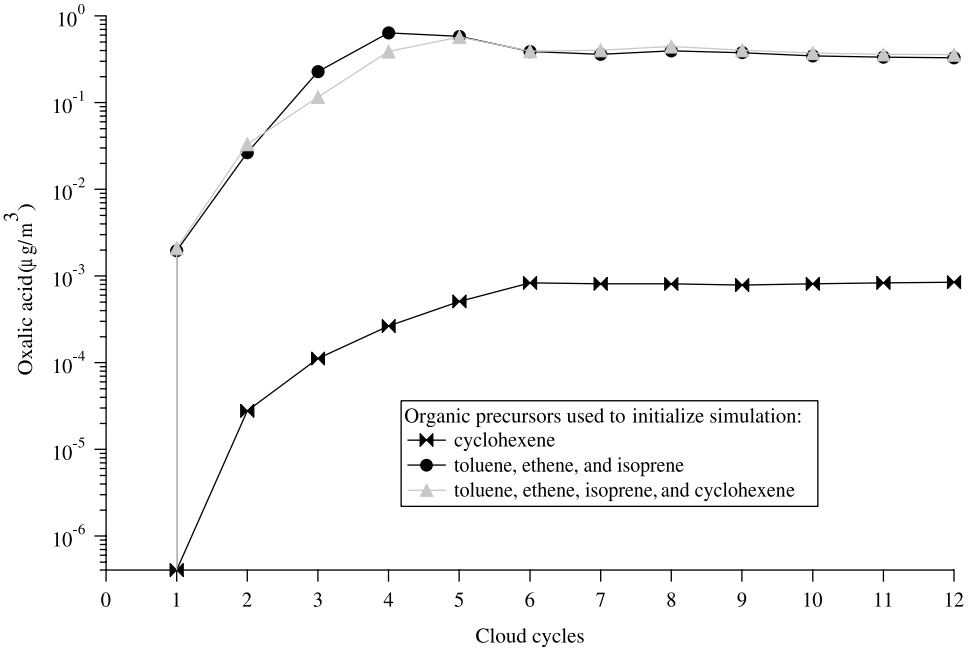

Figure 12. Contribution of different aqueous-phase pathways to production of oxalic acid.

presence of clouds. Both masses evolved chemically in clouds while being transported away from the power plant. Oxalate reached some of its highest levels on this particular flight presumably because of the elevated LWC in the clouds and abundance of clouds in a stratified deck allowing for additional cloud processing time.

[48] A chemical cloud parcel model, initialized with measured aerosol size distributions, gas-phase concentrations, and meteorological conditions, predicted the same relative magnitudes of oxalic acid and SO_4^{2-} production as those measured in the field. Agreement between measurements and predictions for the growth of glyoxylate, malonate, pyruvate, and glutarate lends further support to the aqueous-phase mechanism. The production of oxalic acid is less sensitive to the initial concentration of its gas-phase precursors as compared to production of SO_4^{2-}; this may be a result of the complex multistep nature of oxalic acid production, which leads to the production of volatile side-product species and the depletion of its main aqueous-phase oxidant, OH, by competing reactions. Oxalic acid production is shown to be enhanced with increasing amounts of both LWC and pH in droplets. On the basis of a state-of-the-art aqueous-phase chemical mechanism, the oxidation of glyoxylic acid dominates over that of longer-chain dicarboxylic acids in the production of oxalic acid.

[49] **Acknowledgments.** This work was supported by the National Science Foundation grant ATM-0340832. Graham Feingold and Barbara Ervens were supported by NOAA's Climate Goal. Elliot L. Atlas acknowledges support from the NOAA Office of Global Programs and NOAA Health of the Atmosphere Program. We thank Kurt Anlauf, Art Tham, and Maurice Watt of the Meteorological Service of Canada for providing hydrogen peroxide measurements. Appreciation is extended to William C. Conant for helpful discussions.

References

Blando, J. D., and B. J. Turpin (2000), Secondary organic aerosol formation in cloud and fog droplets: A literature evaluation of plausibility, *Atmos. Environ.*, *34*, 1623–1632.

Brooks, S. D., M. E. Wise, M. Cushing, and M. A. Tolbert (2002), Deliquescence behavior of organic/ammonium sulfate aerosol, *Geophys. Res. Lett.*, *29*(10), 1917, doi:10.1029/2002GL014733.

Chebbi, A., and P. Carlier (1996), Carboxylic acids in the troposphere, occurrence, sources, and sinks: A review, *Atmos. Environ.*, *30*, 4233–4249.

Crahan, K. K., D. Hegg, D. S. Covert, and H. Jonsson (2004), An exploration of aqueous oxalic acid production in the coastal marine atmosphere, *Atmos. Environ.*, *38*, 3757–3764.

Cruz, C. N., and S. N. Pandis (1998), The effect of organic coatings on the cloud condensation nuclei activation of inorganic atmospheric aerosol, *J. Geophys. Res.*, *103*(D11), 13,111–13,123.

Ervens, B., G. Feingold, G. J. Frost, and S. M. Kreidenweis (2004), A modeling study of aqueous production of dicarboxylic acids: 1. Chemical pathways and speciated organic mass production, *J. Geophys. Res.*, *109*, D15205, doi:10.1029/2003JD004387.

Faust, B. C. (1994), Photochemistry of clouds, fogs, and aerosols, *Environ. Sci. Technol.*, *28*, A217–A222.

Feingold, G., S. M. Kreidenweis, and Y. Zhang (1998), Stratocumulus processing of gases and cloud condensation nuclei: 1. Trajectory ensemble model, *J. Geophys. Res.*, *103*((D16)), 19,527–19,542.

Grosjean, D., and K. Fung (1984), Hydrocarbons and carbonyls in Los Angeles air, *J. Air Pollut. Control Assoc.*, *34*, 537–543.

Hegg, D. A., S. Gao, and H. Jonsson (2002), Measurements of selected dicarboxylic acids in marine cloud water, *Atmos. Res.*, *62*, 1–10.

Hegg, D. A., D. S. Covert, P. A. Covert, and H. Jonsson (2005), Determination of the efficiency of an aircraft aerosol inlet, *Aerosol Sci. Technol.*, *39*, 966–971.

Jayne, J. T., D. C. Leard, X. F. Zhang, P. Davidovits, K. A. Smith, C. E. Kolb, and D. R. Worsnop (2000), Development of an aerosol mass spectrometer for size and composition analysis of submicron particles, *Aerosol Sci. Technol.*, *33*, 49–70.

Kalberer, M., J. Yu, D. R. Cocker, R. C. Flagan, and J. H. Seinfeld (2000), Aerosol formation in the cyclohexene-ozone system, *Environ. Sci. Technol.*, *34*, 4894–4901.

Kawamura, K., and K. Ikushima (1993), Seasonal changes in the distribution of dicarboxylic acids in the urban atmosphere, *Environ. Sci. Technol.*, *27*, 2227–2235.

Kawamura, K., and I. R. Kaplan (1987), Motor exhaust emissions as a primary source for dicarboxylic acids in Los Angeles ambient air, *Environ. Sci. Technol.*, *21*, 105–110.

Kawamura, K., and F. Sakaguchi (1999), Molecular distributions of water soluble dicarboxylic acids in marine aerosols over the Pacific Ocean including tropics, *J. Geophys. Res.*, *104*(D3), 3501–3509.

Kawamura, K., H. Kasukabe, O. Yasui, and L. A. Barrie (1995), Production of dicarboxylic acids in the Arctic atmosphere at polar sunrise, *Geophys. Res. Lett.*, *22*, 1253–1256.

Kawamura, K., R. Sempéré, Y. Imai, Y. Fujii, and M. Hayashi (1996), Water soluble dicarboxylic acids and related compounds in Antarctic aerosols, *J. Geophys. Res.*, *101*(D13), 18,721–18,728.

Kawamura, K., N. Umemoto, M. Mochida, T. Bertram, S. Howell, and B. J. Huebert (2003), Water-soluble dicarboxylic acids in the tropospheric aerosols collected over east Asia and western North Pacific by ACE-Asia C-130 aircraft, *J. Geophys. Res.*, *108*(D23), 8639, doi:10.1029/2002JD003256.

Kawamura, K., Y. Imai, and L. A. Barrie (2005), Photochemical production and loss of organic acids in high Arctic aerosols during long-range transport and polar sunrise ozone depletion events, *Atmos. Environ.*, *39*, 599–614.

Kerminen, V. M., K. Teinila, R. Hillamo, and T. Makela (1999), Size-segregated chemistry of particulate dicarboxylic acids in the Arctic atmosphere, *Atmos. Environ.*, *33*, 2089–2100.

Kerminen, V. M., C. Ojanen, T. Pakkanen, R. Hillamo, M. Aurela, and J. Merilainen (2000), Low-molecular-weight dicarboxylic acids in an urban and rural atmosphere, *J. Aerosol Sci.*, *31*, 349–362.

Khwaja, H. A., S. Brudnoy, and L. Husain (1995), Chemical characterization of 3 summer cloud episodes at Whiteface Mountain, *Chemosphere*, *31*, 3357–3381.

Kumar, P. P., K. Broekhuizen, and J. P. D. Abbatt (2003), Organic acids as cloud condensation nuclei: Laboratory studies of highly soluble and insoluble species, *Atmos. Chem. Phys.*, *3*, 509–520.

Leitner, N. K. V., and M. Dore (1997), Mechanism of the reaction between hydroxyl radicals and glycolic, glyoxylic, acetic and oxalic acids in aqueous solution: Consequence on hydrogen peroxide consumption in the H_2O_2/UV and O_3/H_2O_2 systems, *Water Res.*, *31*, 1383–1397.

Lim, H. J., A. G. Carlton, and B. J. Turpin (2005), Isoprene forms secondary organic aerosol through cloud processing: Model simulations, *Environ. Sci. Technol.*, *39*, 4441–4446.

Limbeck, A., and H. Puxbaum (1999), Organic acids in continental background aerosols, *Atmos. Environ.*, *33*, 1847–1852.

Limbeck, A., and H. Puxbaum (2000), Dependence of in-cloud scavenging of polar organic aerosol compounds on the water solubility, *J. Geophys. Res.*, *105*(D15), 19,857–19,867.

Liu, P. S. K., W. R. Leaitch, C. M. Banic, S. M. Li, D. Ngo, and J. W. Megaw (1996), Aerosol observations at Chebogue Point during the 1993 North Atlantic Regional Experiment: Relationships among cloud condensation nuclei, size distribution, and chemistry, *J. Geophys. Res.*, *101*(D22), 28,971–28,990.

Loflund, M., A. A. Kasper-Giebl, B. Schuster, H. Giebl, R. Hitzenberger, and H. Puxbaum (2002), Formic, acetic, oxalic, malonic and succinic acid concentrations and their contribution to organic carbon in cloud water, *Atmos. Environ.*, *36*, 1553–1558.

Mochida, M., N. N. Umemoto, K. Kawamura, and M. Uematsu (2003), Bimodal size distribution of C_2-C_4 dicarboxylic acids in the marine aerosols, *Geophys. Res. Lett.*, *30*(13), 1672, doi:10.1029/2003GL017451.

Norton, R. B., J. M. Roberts, and B. J. Huebert (1983), Tropospheric oxalate, *Geophys. Res. Lett.*, *10*(7), 517–520.

Pakkanen, T. A., K. Loukkola, C. H. Korhonen, M. Aurela, T. Makela, R. E. Hillamo, P. Aarnio, T. Koskentalo, A. Kousa, and W. Maenhaut (2001), Sources and chemical composition of atmospheric fine and coarse particles in the Helsinki area, *Atmos. Environ.*, *35*, 5381–5391.

Poore, M. W. (2000), Oxalic acid in PM2.5 particulate matter in California, *J. Air Waste Manage. Assoc.*, *50*, 1874–1875.

Puxbaum, H., J. Rendl, R. Allabashi, L. Otter, and M. C. Scholes (2000), Mass balance of the atmospheric aerosol in a South African subtropical savanna (Nylsvley, May 1997), *J. Geophys. Res.*, *105*(D16), 20,697–20,706.

Rohrl, A., and G. Lammel (2001), Low molecular weight dicarboxylic acids and glyoxylic acid: Seasonal and air mass characteristics, *Environ. Sci. Technol.*, *35*, 95–101.

Salam, A., H. Bauer, K. Kassin, S. M. Ullah, and H. Puxbaum (2003a), Aerosol chemical characteristics of a mega-city in Southeast Asia (Dhaka-Bangladesh), *Atmos. Environ.*, *37*, 2517–2528.

Salam, A., H. Bauer, K. Kassin, S. M. Ullah, and H. Puxbaum (2003b), Aerosol chemical characteristics of an island site in the Bay of Bengal (Bhola-Bangladesh), *J. Environ. Monit.*, *5*, 483–490.

Saxena, P., and L. M. Hildemann (1996), Water-soluble organics in atmospheric particles: A critical review of the literature and application of thermodynamics to identify candidate compounds, *J. Atmos. Chem.*, *24*, 57–109.

Seinfeld, J. H., and S. N. Pandis (1998), *Atmospheric Chemistry and Physics*, Wiley-Interscience, Hoboken, N. J.

Shantz, N. C., et al. (2004), Chemical and physical observations of particulate matter at Golden Ears Provincial Park from anthropogenic and biogenic sources, *Atmos. Environ.*, *38*, 5849–5860.

Sorooshian, A., F. J. Brechtel, Y. Ma, R. J. Weber, A. Corless, R. C. Flagan, and J. H. Seinfeld (2006), Modeling and characterization of a particle-into-liquid sampler (PILS), *Aerosol Sci. Technol.*, *40*, 396–409.

Squires, P., and J. S. Turner (1962), An entraining jet model for cumulonimbus updraughts, *Tellus*, *14*, 422–434.

Tong, C. H., M. Blanco, W. A. Goddard III, and J. H. Seinfeld (2004), Thermodynamic properties of multifunctional oxygenates in atmospheric aerosols from quantum mechanics and molecular dynamics: Dicarboxylic acids, *Environ. Sci. Technol.*, *38*, 3941–3949.

Turekian, V. C., S. A. Macko, and W. C. Keene (2003), Concentrations, isotopic compositions, and sources of size-resolved, particulate organic carbon and oxalate in near-surface marine air at Bermuda during spring, *J. Geophys. Res.*, *108*(D5), 4157, doi:10.1029/2002JD002053.

Wang, J., R. C. Flagan, and J. H. Seinfeld (2003), A differential mobility analyzer (DMA) system for submicron aerosol measurements at ambient relative humidity, *Aerosol Sci. Technol.*, *37*, 46–52.

Warneck, P. (2003), In-cloud chemistry opens pathway to the formation of oxalic acid in the marine atmosphere, *Atmos. Environ.*, *37*, 2423–2427.

Weathers, K. C., et al. (1988), Cloudwater chemistry from 10 sites in North America, *Environ. Sci. Technol.*, *22*, 1018–1026.

Weber, R. J., D. Orsini, Y. Daun, Y. N. Lee, P. J. Klotz, and F. J. Brechtel (2001), A particle-into-liquid collector for rapid measurement of aerosol bulk chemical composition, *Aerosol Sci. Technol.*, *35*, 718–727.

Yao, X. H., C. K. Chan, M. Fang, S. Cadle, T. Chan, P. Mulawa, K. B. He, and B. M. Ye (2002a), The water-soluble ionic composition of PM2.5 in Shanghai and Beijing, China, *Atmos. Environ.*, *36*, 4223–4234.

Yao, X. H., M. Fang, and C. K. Chan (2002b), Size distributions and formation of dicarboxylic acids in atmospheric particles, *Atmos. Environ.*, *36*, 2099–2107.

Yao, X. H., A. P. S. Lau, M. Fang, C. K. Chan, and M. Hu (2003), Size distributions and formation of ionic species in atmospheric particulate pollutants in Beijing, China: 2-dicarboxylic acids, *Atmos. Environ.*, *37*, 3001–3007.

Yao, X. H., M. Fang, C. K. Chan, K. F. Ho, and S. C. Lee (2004), Characterization of dicarboxylic acids in PM2.5 in Hong Kong, *Atmos. Environ.*, *38*, 963–970.

Yu, J. Z., S. F. Huang, J. H. Xu, and M. Hu (2005), When aerosol sulfate goes up, so does oxalate: Implication for the formation mechanisms of oxalate, *Environ. Sci. Technol.*, *39*, 128–133.

E. L. Atlas, Division of Marine and Atmospheric Chemistry, Rosenstiel School of Marine and Atmospheric Science, University of Miami, Miami, FL 33149, USA.

R. Bahreini, G. Feingold, and J. S. Holloway, Earth System Research Laboratory/Chemical Sciences Division, NOAA, Boulder, CO 80305, USA.

F. J. Brechtel, R. C. Flagan, S. M. Murphy, J. H. Seinfeld, A. Sorooshian, and V. Varutbangkul, Departments of Environmental Science and Engineering and Chemical Engineering, California Institute of Technology, Pasadena, CA 91125, USA. (seinfeld@caltech.edu)

G. Buzorius and H. Jonsson, Center for Interdisciplinary Remotely Piloted Aircraft Studies, Naval Postgraduate School, Marina, CA 93933, USA.

B. Ervens, Department of Atmospheric Science, Colorado State University, Fort Collins, CO 80523, USA.